Smart Structures and Systems, *Vol. 15, No. 3 (2015) 505-522*
DOI: http://dx.doi.org/10.12989/sss.2015.15.3.505

Mechanisms of thermally induced deflection of a long-span cable-stayed bridge

Yi Zhou[1a], Limin Sun[*1] and Zhijian Peng[2b]

[1]*State Key Lab for Disaster Reduction in Civil Engineering, Tongji University, Shanghai, 200092, P.R. China*
[2]*Shanghai Highway Investment Construction & Development Co., Ltd., Shanghai, 200335, P.R. China*

(Received October 27, 2014, Revised January 15, 2015, Accepted January 22, 2015)

Abstract. Variation of temperature is a primary environmental factor that affects the behavior of structures. Therefore, understanding the mechanisms of normal temperature-induced variations of structural behavior would help in distinguishing them from anomalies. In this study, we used the structural health monitoring data of the Shanghai Yangtze River Bridge, a steel girder cable-stayed bridge, to investigate the mechanisms of thermally induced vertical deflection (D_T) at mid-span of such bridges. The D_T results from a multisource combination of thermal expansion effects of the cable temperature (T_{Cab}), girder temperature (T_{Gir}), girder differential temperature (T_{Dif}), and tower temperature (T_{Tow}). It could be approximated by multiple linear superpositions under operational conditions. The sensitivities of D_T of the Shanghai Yangtze River Bridge to the above temperatures were in the following order: $T_{Cab} > T_{Gir} > T_{Tow} > T_{Dif}$. However, the direction of the effect of T_{Cab} was observed to be opposite to that of the other three temperatures, and the magnitudes of the effects of T_{Cab} and T_{Gir} were found to be almost one order greater than those of T_{Dif} and T_{Tow}. The mechanisms of the thermally induced vertical deflection variation at mid-span of a cable-stayed bridge as well as the analytical methodology adopted in this study could be applicable for other long-span cable-stayed bridges.

Keywords: cable-stayed bridge; temperature effect; mid-span deflection; mechanisms; structural health monitoring

1. Introduction

Bridges constitute a key role in a modern transportation system and their operational conditions have always been of great concern to bridge owners, users, and engineers. Structural health monitoring (SHM) technology enables long-term, continuous, and on-site measurement of the impact of environmental and loading conditions on a bridge. Consequently, a large number of SHM systems have emerged over the last two decades, almost all of which utilize features or indices extracted from measurements in detecting damages or anomalies (Boller *et al*. 2009). However, it is widely recognized that most structural condition indices vary with environmental factors, especially the temperature conditions. Hence, for more reliable structural evaluation, it is necessary to study thermal effects and how to cancel them out (Catbas *et al.* 2008, Deng *et al*.

*Corresponding author, Professor, E-mail: lmsun@tongji.edu.cn
[a] Ph.D. student, E-mail: zhouyi8659@126.com
[b] Chief Engineer, E-mail: pengzhijian@shgltz.com

http://www.techno-press.org/?journal=sss&subpage=8 ISSN: 1738-1584 (Print), 1738-1991 (Online)

2010, Gentile and Saisi 2013, Li *et al*. 2010, Magalhães *et al*. 2012, Moorty and Roeder 1992, Ni *et al*. 2011, Reynders *et al*. 2013, Sohn 2007, Wang 2009, Wenzel 2009). In this study, the authors investigated the relationship between the temperature and mid-span deflection of a long-span cable-stayed bridge, which is a basic performance indicator of the global rigidity and mechanical state of such a bridge.

During design phase of a bridge structure, the thermally induced vertical deflection at mid-span of bridge girder, denoted as D_T, is considered under the limit states, which do not represent structural behavior under normal operation. Field measurements are therefore undoubtedly the best method for investigating actual structures in the real-world. Barr *et al*. (2000), Burdet (2010), and Ghali *et al*. (2000) undertook long-term observations of the mid-span deflection of short and medium span girder bridges and considered the temperature gradient over the girder depth to be the main reason for variations in the deflection. Figueiras *et al*. (2005) also observed that the crown of a centenary arch bridge in Portugal curved upward with increasing temperature.

Thermal effects are not only due to temperature variations, but also to structural constraints. Owing to the complex system of a cable-supported bridge, its thermal effects are of particular interest. Studies on the famous Tsing Ma Suspension Bridge conducted by Xu *et al*. (2010) and Xia *et al*. (2013) revealed that the thermally induced vertical deflection at mid-span decreased with increasing temperature, and that the seasonal variation of D_T was much wider than that during a summer day. Xu *et al*. (2010) concluded that the D_T of the 1377-m-span suspension bridge was partially dominated by the deformation of the main cables. Another often cited SHM campaign on the Tamar Suspension Bridge in the UK, which was transformed into a hybrid cable-stayed and suspension bridge after its upgrade, revealed that a temperature increase caused a downward movement of the mid-span (Brownjohn *et al*. 2009, Koo *et al*. 2013). Based on a multiple linear regression analysis and subsequent comparison of regression coefficients, Westgate (2012) posited that the D_T of the 335-m-span Tamar Bridge was mainly affected by the elongation of the suspension cables. There have also been reports of the D_T of suspension bridges such as the Akashi Kaikyo Bridge (Katsuchi *et al*. 2008), the Yangluo Yangtze River Bridge (Li *et al*. 2011), and the Yeongjong Bridge (Kim *et al*. 2005), which have central spans of 1991, 1280, and 300 m, respectively. As with the two earlier mentioned bridges, the thermally induced vertical deflections at mid-span of these three bridges occur downward with increasing temperature.

Cable-stayed bridges with multi-cable systems are highly statically indeterminate and their inter-constraints are stronger than those of suspension bridges, resulting in more complex thermal effects. Cao *et al*. (2011) analyzed the D_T of the Zhanjiang Bay Bridge, a cable-stayed bridge with a 480-m central steel box girder span, over a period of five summer days. Unlike most other observations, the central span of the girder curved upward under high afternoon temperatures. This was attributed to the uniform temperature increase of the entire structure and/or the localized temperature increase of the top plate of the girder. However, the variation of the D_T over the seasonal cycle was not covered. Moreover, no temperature sensors were placed on the external surface of the towers. Thus the tower temperature used for the finite element (FE) model was highly uncertain. Li (2012) explored the thermally induced vertical deflection at mid-span of the Donghai Bridge, a cable-stayed bridge spanning 420 m and with a steel-concrete composite section girder, and obtained the data range between March and September 2007. The mid-span of the bridge exhibited a slight downward deflection with increasing effective temperature of the girder. The time lags between the deflection and the temperature were also observed. Although an ARX model for predicting the D_T was developed, the physical explanation of such a model was

not considered in the modeling process. Zhu *et al*. (2006) and Chen *et al*. (2006) respectively presented and modeled the same nine-day winter measurements on the Dafosi Yangtze River Bridge, a 450-m-span concrete cable-stayed bridge. It was observed that an increase in the temperature was accompanied by a downward movement at mid-span. An artificial neural network was used to reproduce the winter D_T measurements, but the model was not verified for summer measurements.

From the extensive previous works mentioned so far, it appears that all suspension bridges display similar characteristics, namely a downward thermally induced vertical deflection at mid-span with increasing temperature. However, the direction of the D_T of a cable-stayed bridge depends on the specific bridge; some bridges curve upward mid-span with increasing temperature, whereas others curve downward. Generally, the D_T of a cable-stayed bridge is much more complex and the underlining mechanism is not yet explicitly understood. Moreover, a preliminary study of the field measured D_T of the Shanghai Yangtze River Bridge found that it was difficult to simultaneously explain the seasonal and daily variations of the thermally induced vertical deflection at mid-span based on the air temperature or the temperature of a certain structural component. Hence, it is desirable to determine the mechanisms of variation of D_T using the field SHM data.

The rest of this paper consists of five parts. Section 2 presents the field measurements of the temperature and mid-span deflection of the Shanghai Yangtze River Bridge in February and July 2012. In Section 3, the possible reasons for the D_T variation are discussed qualitatively; and followed by an FE analysis in Section 4 to quantify the effects of the cable temperature (T_{Cab}), girder temperature (T_{Gir}), girder differential temperature (T_{Dif}), tower temperature (T_{Tow}), and temperature-dependent elastic moduli on the thermally induced vertical deflection at mid-span. Section 5 explains the monitoring results and compares the thermal effects of different mechanisms. The findings of this study do not only advance an understanding of the thermal effects on cable-stayed bridges, but also provide theoretic and measured bases for the design and evaluation of such bridges.

2. Monitoring results

2.1 Shanghai Yangtze River Bridge and its SHM system

The Shanghai Yangtze River Bridge is located on the outskirt of Shanghai City, China, at the southern fringe of the north subtropical zone. It is a five-span cable-stayed bridge with dual towers, dual cable planes, and a separated double-box steel girder. It has a span arrangement of 92 m + 258 m + 730 m + 258 m + 92 m = 1430 m and was opened to traffic on October 31, 2009 (Shao 2010). The SHM system of the bridge includes 227 sensors, which are used for real-time monitoring of the environmental and loading conditions as well as the static and dynamic responses of the bridge (Sun *et al*. 2010). The structural temperature and the mid-span deflection are respectively measured by Fiber Bragg Grating (FBG) temperature sensors and GPS technology, with sampling intervals of 1 min and 0.1 s, respectively. In this paper, the D_T is the vertical position or level at the middle of the central span, and the reference is assumed to be the elevation at the time of installing the sensor. A positive value indicates upward movement of the girder. The Shanghai Yangtze River Bridge forms a floating system along its longitudinal axis; it does not

have vertical bearings at the intersections of the girder and the tower. Unlike a monolithic girder-pier system, the thermal effects of the side piers and the subsidiary piers of the Shanghai Yangtze River Bridge, on which no temperature sensors were installed, have little effect on the superstructure. Hence, the temperature changes on those piers as well as the settlement at all the bases are neglected.

2.2 Characteristics of temperature field

The thermally induced vertical deflection at mid-span is a consequence of structural temperature distribution. In this paper, the measured temperatures are introduced into the FE model directly. This is done instead of a transient heat transfer analysis, which is highly uncertain with respect to the unmeasured heat boundary conditions, e.g., the intensity of solar radiation. Hence, it is necessary to first explore the temperature distribution. The ambient air temperature has two dominant cycles, a seasonal and a daily one. To take both cycles into consideration, measurements obtained in February and July, respectively the coldest and warmest months in 2012, were analyzed. The data for the individual months reflected the daily variations of the temperature and D_T, whereas comparison of the data for winter and summer reflected the seasonal variations. The relationships between the ambient temperature and the structural temperature for different structural components and during winter and summer are quite different. Only the distribution of the structural temperature is discussed below, using the data for February 19 and July 24 as examples. The hourly averaged temperature is used because of its slow variation.

2.2.1 Longitudinal temperature distribution of the girder

The temperatures at different sections of the top and bottom decks along the main girder vary at almost the same rate towards their peaks and troughs. Fig. 1 shows the longitudinal temperature distributions of the top and bottom decks of the steel box girder at the time of the peak temperature of the top plate on July 24 and the time of the trough temperature on February 19. It should be noted that the longitudinal temperature field is almost uniform along the girder, with the exception of the temperatures at both tower-girder intersections, which are a little lower than those of the other three sections. This is due to shading of the towers during the daytime. Without consider the difference of the baseline, the temperature distribution at the time of peak temperature on February 19 would be similar to that on July 24, and both would have a positive vertical temperature difference. Likewise, the temperature distributions at the trough temperature times on February 19 and July 24 are similar, although there is a negative temperature difference and its magnitude is much smaller than the positive difference for the peak temperature times. Hence, the following FE analysis considers the vertical temperature gradient but ignores the longitudinal gradient.

2.2.2 Temperature distribution in mid-span section of the girder

The structural temperature distribution at the mid-span section (Fig. 2) shows that the lateral thermal gradient is diminutive at both the peak and trough temperature times. The two outermost temperature sensors on the top plate were located just beneath the safety barriers on the deck, which might account for their readings being lower than those of the other four sensors on the top plate. Consequently, the average of the four sensors is used as the representative temperature of the top plate for the FE analysis, in which the lateral thermal gradient is also ignored.

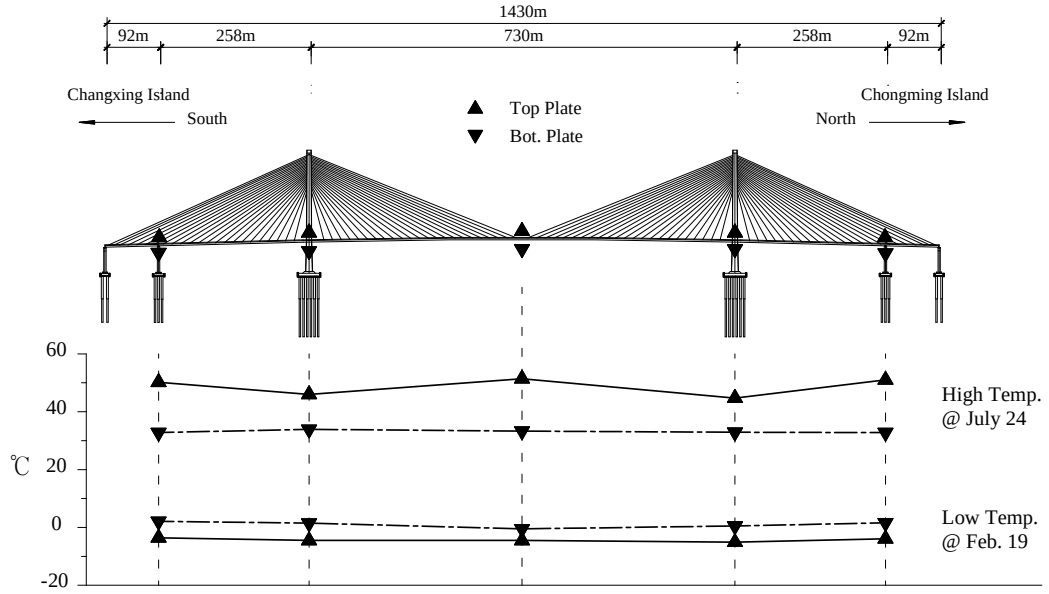

Fig. 1 Bridge's Elevation view and measured longitudinal temperature distribution of girder

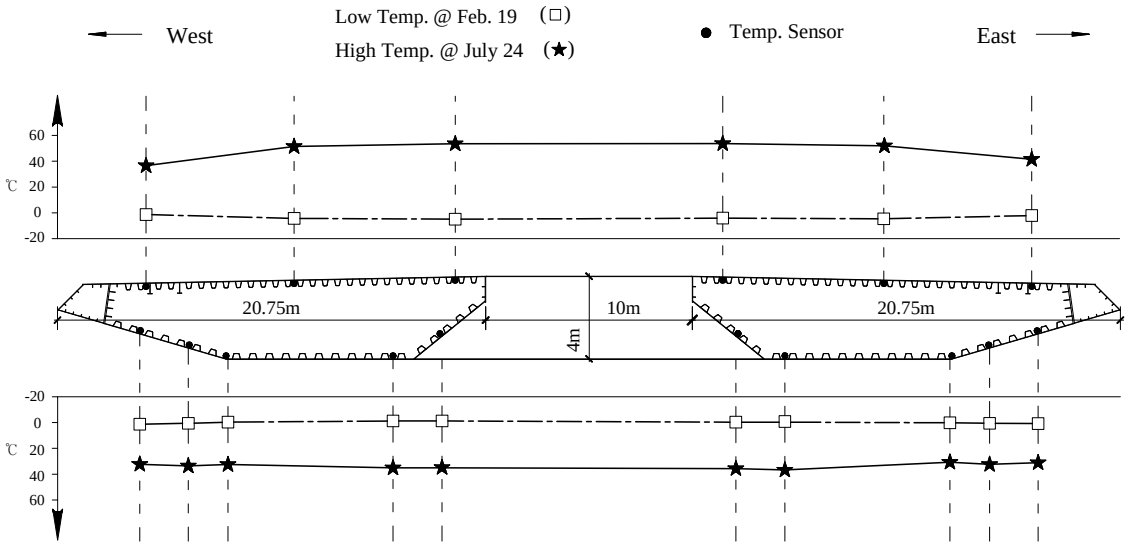

Fig. 2 Measured temperature distribution at mid-span section of girder

2.2.3 Tower temperature

The temperature of each concrete tower was monitored in one section at about midway along its height. The temperature evolutions of both towers were much similar and the interior temperatures were very stable with almost no daily variation. However, their external surface

temperature gradients were not negligible due to the effect of direct sunlight (Figs. 3 and 4). Based on the measurements, it is reasonable to assume in the FE model that both towers have identical temperature fields, which are uniform along their height. The thermal difference between the external north and south faces should be considered, whereas the internal temperatures can be neglected.

2.2.4 Cable temperature

All mearsured cables of the Shanghai Yangtze River Bridge have similar temperature variation trends. Fig. 5 shows the temperatures of the four longest cables of the center span, the mean of which is used to represent the temperature of all the stay-cables in the FE model, neglecting the temperature gradient along the cable length. It is necessary to note that the temperature sensors were installed on the cable surface rather than inside them. Hence, the measurements might differ from the actual temperatures of the steel wires.

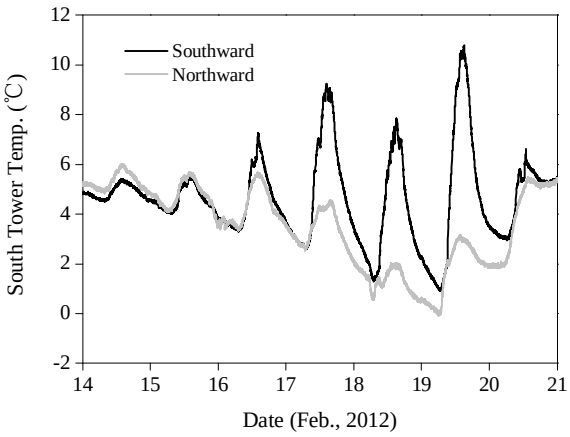

Fig. 3 Temperature of outer surfaces of south tower

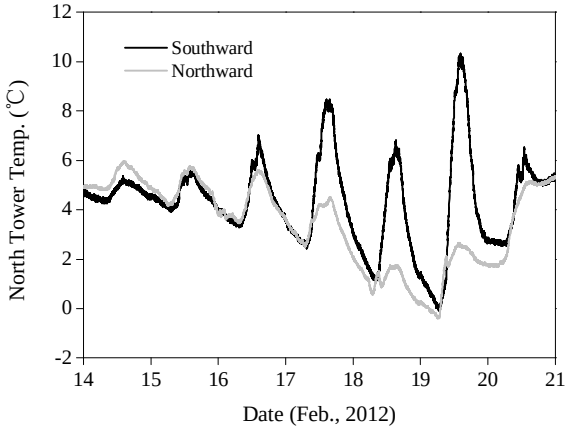

Fig. 4 Temperature of outer surfaces of north tower

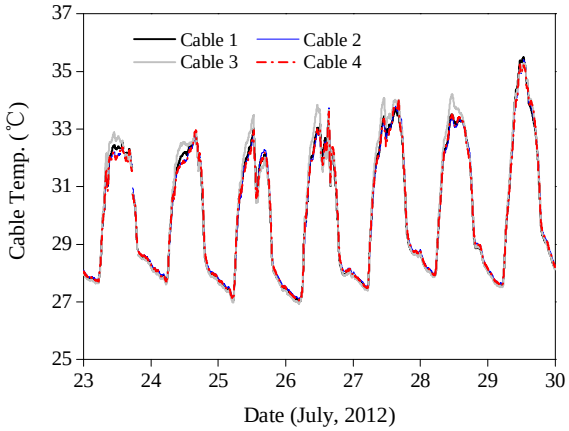

Fig. 5 Temperatures of four longest cables in center span

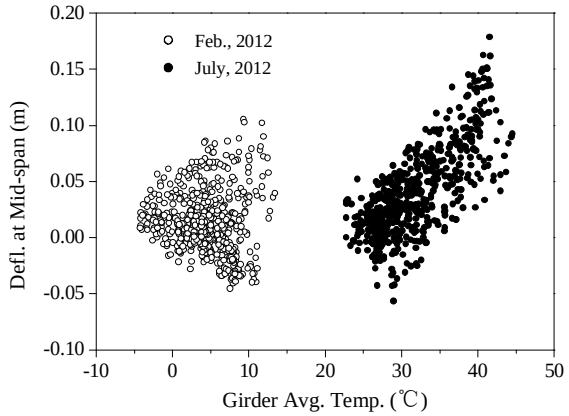

Fig. 6 D_T vs. T_{Gir}

2.3 Measured D_T

Compared to the effect of traffic, the thermally induced vertical deflection variation at mid-span is rather slow and can be represented by the hourly average of the measured deflections. Fig. 6 is a scatter plot of D_T versus T_{Gir} for two months. In July, an upward movement at the mid-span occurred with increasing girder temperature T_{Gir}. This is in agreement with the observation of Cao *et al*. (2011), but in conflict with those of Zhu *et al*. (2006) and Li (2012). However, in February, the D_T did not correlate well with the T_{Gir}. Moreover, the positions of the girder in February and July were almost the same. Hence, on an annual scale, the observation of an upward D_T with increasing temperature is very vague compared to that in July. Fig. 6 suggests that the girder temperature may not be the only factor that affects the D_T. In the next two sections, the authors discuss five mechanisms of D_T variation.

3. Mechanisms of D_T variation

Here we discuss five possible mechanisms of the thermally induced vertical deflection variation at mid-span, which correspond to the effects of the cable temperature T_{Cab}, girder temperature T_{Gir}, girder differential temperature T_{Dif}, tower temperature T_{Tow}, and variation of the material elastic modulus E. Considering a temperature increase as an example, Fig. 7 illustrates the five mechanisms. For simplicity, the vertical constraints on the sides of the bridge and the subsidiary piers are not shown.

3.1 Mechanism 1: cable temperature

The elongation of the cable due to increase in temperature lowers the girder mid-span (Fig. 7(a)).

3.2 Mechanism 2: girder temperature

The T_{Gir} indirectly affects the D_T. As the temperature increases, the girder expands at both ends, and then both towers move apart due to the cable constraints; this eventually raises the mid-span of the girder (Fig. 7(b)).

3.3 Mechanism 3: girder differential temperature

The T_{Dif} of the Shanghai Yangtze River Bridge's girder could exceed 20°C due to sunlight, resulting in curvature of the girder in the vertical plane. A cable-stayed bridge is analogous to an elastically supported continuous beam; hence, the magnitude and direction of the D_T depend on the number of spans. A question mark is therefore used to indicate the uncertainty of D_T direction in Fig. 7(c).

3.4 Mechanism 4: tower temperature

The tower height varies with the T_{Tow}, resulting in a change in the D_T (Fig. 7(d)). Moreover, the temperature difference between the north and south surfaces of the towers causes asymmetric deformation and therefore has little effect on the D_T of the girder. This is why the temperature difference of tower is not considered here.

3.5 Mechanism 5: change in elastic moduli

According to Xia *et al*. (2012), the temperature-dependent elastic moduli are the dominant cause of change in structural frequency with temperature. For unit temperature increase, the elastic moduli of steel and concrete decrease by 0.036% and 0.30%, respectively. Consequently, decreases in the elastic moduli of steel and concrete with increasing temperature also reduce the structural stiffness, thereby reducing the D_T (Fig. 7(e)).

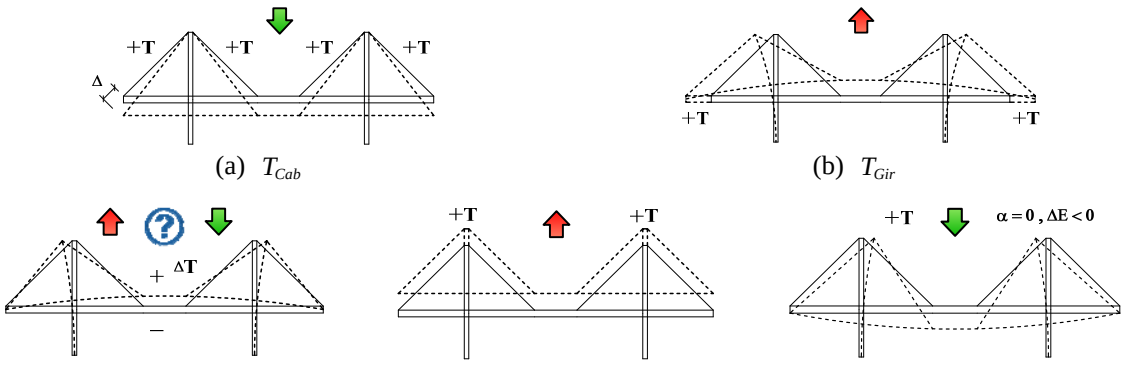

(a) T_{Cab} (b) T_{Gir}

(c) T_{Dif} (d) T_{Tow} (e) E variation

Fig. 7 Schematic diagrams of five D_T variation mechanisms

4. FE analysis

In this section, we develop an FE model for quantifying the sensitivities of the five mechanisms of the thermally induced vertical deflection variation at mid-span discussed in Section 3.

4.1 FE model and assumptions

The Shanghai Yangtze River Bridge is idealized as a 3D beam-element model with double girders, comprising 1673 elements and 1805 nodes (Fig. 8). Each cable is simulated by one element, the elastic modulus of which is modified by the Ernst formula (Eq. (1)) with the consideration of the sag effect.

$$E_{eq} = \frac{E_0}{1 + \frac{A_0 \cdot q^2 \cdot l^2}{12 \cdot F^3} E_0} \tag{1}$$

where E_{eq} is the equivalent elastic modulus of cables, E_0 is the initial modulus of cables, A_0 is the section area of cables, q is the self-weight of cables per unit length, l is cables' horizontal projection length, and F is the tension force in cables, which is set to the design tension. The variations of E_{eq} which result from the changing tension F and from the changing initial modulus E_0 are proven to be in the same order of magnitude. Because the thermally induced vertical deflection at mid-span is insensitive to the change of E_0 (see Section 4.3), thus we ignore the change of cables' equivalent elastic moduli with the changing tension.

4.1.1 Temperature loading

Based on the discussion in Subsection 2.2, five structural temperatures are taken into consideration, namely the top and bottom plate temperatures of the girder, the external north and south surface temperatures of the tower, and the cable temperature (see Table 1). The temperature gradient along the depth of both the girder and the tower was assumed to be linear.

Table 1 Temperature load in FE model

°C	Feb. 19 Trough Temp.	Feb. 19 Peak Temp.	July 24 Trough Temp.	July 24 Peak Temp.
Girder Top	-4.5	20.0	26.7	51.6
Girder Bottom	-0.6	5.4	27.8	32.5
Tower South	0.5	10.4	27.4	30.4
Tower North	-0.1	2.7	27.8	29.5
Cable	-1.3	7.2	28.0	32.5

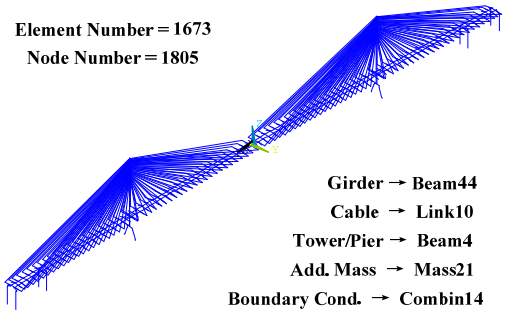

Fig. 8 Information on FE model

4.1.2 Thermal expansion/contraction effect

The effect of the thermal expansion/contraction on the D_T was simulated by introducing the linear thermal expansion coefficients $\alpha_s = 1.2e-5/°C$ and $\alpha_c = 1.0e-5/°C$ for steel and concrete, respectively.

4.1.3 Temperature-dependent elastic moduli

We assumed that the elastic moduli of steel and concrete, respectively denoted by E_S and E_C, vary linearly with temperature at the rates of $\alpha_{Es} = -0.00036/°C$ and $\alpha_{Ec} = -0.00300/°C$, respectively (Xia *et al*. 2012).

4.1.4 Calculation assumption

Due to the unavailability of the initial status of the temperature field and structural responses, the absolute thermal effects for a particular temperature field could not be obtained. Hence, we assumed that the structural thermal responses are a function of the temperature field and independent of the process of heating and cooling. The calculated thermal effects for a particular temperature field could therefore be defined as the difference between the response of the temperature field and that of a reference state. The applied reference state was a virtual condition in which the entire structure had a uniform temperature of 27°C, which is the air temperature at the girder closure. Actually, the reference state has no effect on the calculating response difference between two measured temperature fields.

4.2 Comparison with measurements

A total of four temperature fields (Table 1) at the peak and trough temperature times on February 19 and July 24 were inputted to the FE model to calculate the seasonal and daily variations of the structural responses and verify the applicability of the FE model. The calculation or measurements for the peak temperature on July 24 minus the counterparts for the trough temperature on February 19 represent the thermal effects on an annual scale, whereas the difference between the responses for the peak and trough temperatures on February 19 or July 24 could reflect the thermal effects on a daily scale for winter and summer, respectively.

In general, good agreement was observed between the calculated and measured thermally induced vertical deflections at mid-span (row A in Table 2). On both the annual and daily scales, the variation trend of the calculated D_T values are the same as that of the measured values (their signs are identical). Quantitatively, the differences between the calculations and measurements are about 9% for the annual change and 6% for the daily change on July 24, both of which are acceptable. The difference for February 19 exceeds 132%, which might be related to the fact that the actual variation of the D_T is small (about 0.05 m).

In addition to the D_T, the variations of the girder length, tower distance, total/elastic strain at both the top and bottom plates at mid-span, and the averaged tension of the four longest cables in the center span were also compared. From Table 2, consistency can be observed in the trends of the variation between the analytical and measurement results, which indicates that the developed FE model could identify the basic trends of the thermally induced responses on both the annual and daily scales. The quantitative deviation of the calculations from the measurements in Table 2 may be due to measurement errors, inaccuracy of the FE model, and approximations of the temperature field.

Table 2 Comparison of thermally induced quantities

			Feb. 19 $\Delta=Day_{High}-Day_{Low}$			July 24 $\Delta=Day_{High}-Day_{Low}$			July 24–Feb. 19 $\Delta=Year_{High}-Year_{Low}$		
			Measured	Analytical	RD* (%)	Measured	Analytical	RD (%)	Measured	Analytical	RD (%)
			(1)	(2)	(3)	(4)	(5)	(6)	(7)	(8)	(9)
A	D_T (m)		0.046	0.107	132.5	0.166	0.176	6.0	0.131	0.119	-8.9
B	Girder Length (m)		0.24	0.24	2.5	0.19	0.23	21.2	0.68	0.73	6.7
C	Tower Distance (m)		0.17	0.11	-38.5	0.18	0.12	-33.1	0.45	0.35	-21.9
D	Total Strain (με)	Top	188.41	179.29	-4.8	177.60	174.03	-2.0	551.87	528.28	-4.3
E		Bot.	162.65	180.58	11.0	135.07	174.82	29.4	486.39	529.55	8.9
F	Elastic Strain (με)	Top	-115.19	-114.71	-0.4	-114.00	-124.77	9.4	-109.33	-144.92	32.6
G		Bot.	109.85	108.58	-1.2	100.27	118.42	18.1	127.29	132.35	4.0
H	Cable Force (kN)		46.83	47.75	2.0	70.00	64.30	-8.1	96.65	74.40	-23.0

*Relative Difference (RD) = (Analytical - Measured)/Measured × 100%

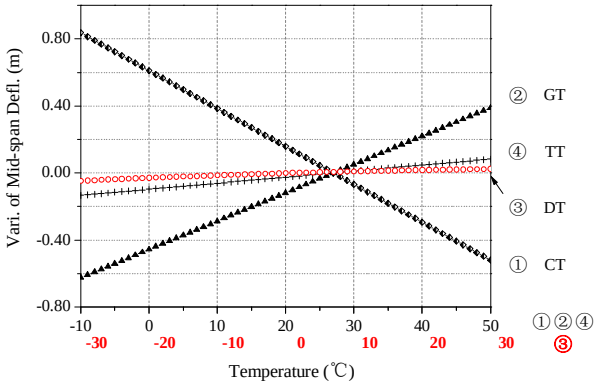

Fig. 9 Calculated D_T for four mechanisms

The total strain ε_M in Table 2 comprises the local deformation of the two parts; i.e., the thermally induced stress-free strain $\varepsilon_T = \alpha_s \cdot \Delta T$ and the elastic strain ε_E: $\varepsilon_M = \varepsilon_T + \varepsilon_E$. In the FE simulation, the temperature change ΔT was obtained as the average of the four sensors on the top or bottom plates (Fig. 2), whereas the measured elastic strain was determined using the value of ΔT of only one temperature sensor. This temperature difference is the reason why the analytical and measured values of the total strain minus the elastic strain in Table 2, which should be equal to $\alpha_s \cdot \Delta T$, are a little different.

After the verification of the FE model, the sensitivities of the five mechanisms of the thermally induced vertical deflection variation mentioned in Section 3 were quantitatively compared by parametric analysis to obtain further insight into the thermal effects.

4.3 Comparison of D_T sensitivities

Using the temperature-dependent elastic moduli of concrete and steel, we calculated the variation of D_T for exclusive changes in each of the mechanisms in Sections 3.1–3.4. Considering real-life possible ranges, the temperature variations for the four mechanisms were separately set as follows: (1) -10–50°C for cable temperature, (2) -10–50°C for girder temperature, (3) -30–30°C for girder differential temperature, and (4) -10–50 °C for tower temperature. Each temperature was varied in steps of 1°C. Particularly for T_{Dif}, the top plate temperature was increased from -15 to 15°C, whereas the bottom plate was decreased from 15 to -15°C, both in steps of 0.5°C. Sixty cases of each mechanism were considered and the corresponding calculated values of the D_T were used to draw the curve in Fig. 9, where the intersection point of all the four separate curves corresponds to the reference temperature 27°C. The relationship of the D_T with each of the four temperatures is almost linear over the normal temperature ranges. The slopes of the four curves represent the sensitivity of the thermally induced vertical deflection at mid-span to the respective temperatures, namely the variation of the D_T per unit temperature rise, which is referred to as the effect coefficient (β) in Table 3. It can be seen from column 2 of Table 3 that the sensitivities of the D_T to the four mechanisms are in the following order: T_{Cab} > T_{Gir} > T_{Tow} > T_{Dif}. Moreover, the level at mid-span decreases with increasing T_{Cab}, but increases with

increasing T_{Gir}, T_{Dif}, and T_{Tow}. Except the T_{Dif}, the directions of the other three temperatures' effects are in agreement with the qualitative judgments in Section 3.

Two calculation procedures were separately considered for the three main components of a cable-stayed bridge for mechanism 5. In Procedure 1, the thermal expansion effect was considered, whereas the elastic moduli changes with temperature were ignored. In Procedure 2, the elastic moduli changes with temperature were considered, whereas the thermal expansion effects were ignored ($\alpha_s = 0$ or $\alpha_c = 0$). The effect coefficients for the two calculation procedures are listed in columns 3 and 4 of Table 3, which indicates that the D_T sensitivity to changes in the elastic moduli is about one or two orders of magnitude less than that for the thermal expansion effect.

Worthy of note is also the fact that the effect coefficients in column 2 of Table 3 are equal to the sum of those in columns 3 and 4. The effects of the thermal expansion coefficient α and the elastic modulus E on the D_T can therefore be approximated by a linear superposition formula within the temperature range of -10–50°C.

The above discussions reveal that the D_T of a cable-stayed bridge is the resultant effect of the thermal expansion/contraction of multiple structural components. However, because of the different temperature ranges experienced by the T_{Cab}, T_{Gir}, T_{Dif}, and T_{Tow} in reality, their effect coefficients cannot be used to account for their actual respective effects on the D_T. These effects will be compared in the next section by considering the actual temperature variation ranges.

5. Discussions

Columns 3, 7, and 11 of Table 4 give the actual variations of the T_{Cab}, T_{Gir}, T_{Dif}, and T_{Tow} based on the measured temperatures at the peak and trough temperature times on February 19 and July 24 (i.e., ΔT_i, i=1−4). Columns 4, 8, and 12 present the product of the effect coefficients and the actual variations: $I_i = \beta_i \times \Delta T_i$, where the sign of I_i indicates the direction of the effect of the i^{th} mechanism on the D_T, and the absolute value $|I_i|$ is the actual effect. For easy comparison, the effects of the four mechanisms on the D_T were normalized by the effect of the T_{Gir}, I_2. The results are given in columns 5, 9, and 13. Furthermore, the contribution of each mechanism to the overall D_T can be estimated using

Table 3 Summary of effect coefficients (β) Unit: m/°C

	Mechanism	Expan./Contr. + E Change	Expan./Contr. only	E Change only
	(1)	(2)	(3)	(4)
A	1: T_{Cab}	**-0.0226**	**-0.0208**	**-0.0018**
B	2: T_{Gir}	**0.0169**	**0.0171**	**-0.0002**
C	3: T_{Dif}	**0.0012**	-	-
D	4: T_{Tow}	**0.0036**	**0.0041**	**-0.0005**

Table 4 Calculated D_T for each mechanism

	Mechanism (i)	β_i (m/°C)	Feb. 19 $\Delta=Day_{High}-Day_{Low}$				July 24 $\Delta=Day_{High}-Day_{Low}$				July 24–Feb. 19 $\Delta=Year_{High}-Year_{Low}$			
			ΔT_i (°C)	I_i (m)	$\lvert I_i\rvert/I_2$ (%)	C_i (%)	ΔT_i (°C)	I_i (m)	$\lvert I_i\rvert/I_2$ (%)	C_i (%)	ΔT_i (°C)	I_i (m)	$\lvert I_i\rvert/I_2$ (%)	C_i (%)
	(1)	(2)	(3)	(4) (2)×(3)	(5)	(6) (4)/Σ_1	(7)	(8) (2)×(7)	(9)	(10) (8)/Σ_2	(11)	(12) (2)×(11)	(13)	(14) (12)/Σ_3
A	1: T_{Cab}	**-0.0226**	8.5	-0.192	74.4	-172.3	4.5	-0.103	41.2	-56.9	33.9	-0.765	101.5	-619.8
B	2: T_{Gir}	**0.0169**	15.3	0.258	100.0	231.7	14.8	0.250	100.0	138.7	44.6	0.754	100.0	610.6
C	3: T_{Dif}	**0.0012**	18.6	0.022	8.5	20.1	20.2	0.024	9.6	13.4	23.0	0.028	3.7	22.4
D	4: T_{Tow}	**0.0036**	6.3	0.023	8.9	20.5	2.4	0.009	3.6	4.8	29.8	0.107	14.2	86.7
E	ΣI_i		Σ_1 = **0.111**			100	Σ_2 = **0.180**			100	Σ_3 = **0.123**			100

5.1 Verification of linear superposition

The summations Σ_1–Σ_3 in row E of Table 4 are very close to the calculated values of D_T in Table 2, the difference being about 3%. In other words, the superposition of the individual thermally induced vertical deflections at mid-span due to the T_{Cab}, T_{Gir}, T_{Dif}, and T_{Tow} is almost equal to the total D_T produced by the four mechanisms together, which indicates that the effects of the four mechanisms on the D_T can be approximated by the linear superposition. This observation is surprising for such a long-span cable-stayed bridge. Additionally, the fact that $\Sigma_3 < \Sigma_2$ in row E shows that it is possible for the seasonal variation of the D_T for a cable-stayed bridge to be less than the daily variation.

5.2 Comparison of effects of four mechanisms

In this subsection, we compare the effects of the T_{Cab}, T_{Gir}, T_{Dif}, and T_{Tow}, taking the actual temperature variation range into consideration. From column 13 in Table 4, the magnitudes of the effects of the T_{Cab} and T_{Gir} are one order larger than the effects of the T_{Dif} and T_{Tow} on the annual scale. However, the effects of these two dominant mechanisms on the D_T are opposite, which makes the contribution of the weakest mechanism, T_{Dif}, to account for 22.4% of the overall D_T variation after offsetting the effects of the T_{Cab} and T_{Gir}. Consequently, none of the four mechanisms can be omitted if a linear superposition model is used to predict the D_T.

From columns 5 and 9 of Table 4, it can be seen that, on the daily scale, the magnitudes of the effects of T_{Cab} and T_{Gir} are one order larger than those of T_{Dif} and T_{Tow}. It is worthy of note that the effect of T_{Gir} is not always greater than that of T_{Cab}, and that the relative importance of T_{Dif} and T_{Tow} is also uncertain. Although the temperature range of different structural

components depends on the weather conditions and the observation times due to the thermal lags, it is hardly possible for the T_{Cab} and T_{Gir} to have less effect than the T_{Dif} and T_{Tow}, which is because their effect coefficients are one order of magnitude larger than those of the latter two mechanisms (see Table 3).

5.3 Explanation of the monitoring results

The effect coefficients in Table 3 were used as the coefficients of a multiple linear formula for simulating the thermally induced vertical deflection at mid-span in accordance with the temperatures measured in February and July as shown in Eq. (3)

$$D_T^a = -0.0226 \cdot T_{Cab} + 0.0169 \cdot T_{Gir} + 0.0012 \cdot T_{Dif} + 0.0036 \cdot T_{Tow} + D_0 \tag{3}$$

where the D_T^a denotes the calculated D_T, and D_0 is a constant related to the initial state. To ensure the same baseline as the measured D_T, the offset D_0 can be estimated using

$$D_0 = Avg\left(D_T\right) - Avg\left(-0.0226 \cdot T_{Cab} + 0.0169 \cdot T_{Gir} + 0.0012 \cdot T_{Dif} + 0.0036 \cdot T_{Tow}\right) \tag{4}$$

where $Avg(\cdot)$ denotes the average operation and D_T is measured in February and July. The scatter plot of D_T^a versus T_{Gir} is shown in Fig. 10, with the original Fig. 6 overlaid. In terms of the distribution pattern of the points, the measured D_T and the simulated D_T^a are similar. The multiple linear formula presented as Eq. (3) can be used to properly explain the variation of the D_T. Furthermore, using the same D_0, Eq. (3) is also applicable to cases in January and August. Generally speaking, this physics-based model can be used to explain the annual and daily variations of the thermally induced vertical deflection at mid-span. Considering that it disregards the time lags and auto-regression of D_T, it can be easily applied in practice.

There was some discrepancy between the measured D_T and the calculated one; e.g., the relationship between the two appeared to be skewed in Fig. 12. It should be noted that the effect coefficients of the T_{Cab}, T_{Gir}, T_{Dif}, and T_{Tow} in Eq. (3) were obtained by an FE model that had not been calibrated using recorded data, which made the errors in the effect coefficients inevitable. Measurement errors and uncertainty of the temperature distribution are also possible reasons for the discrepancy and further studies are required to investigate these issues for more accurate evaluation of the structural conditions.

6. Conclusions

The mid-span deflection of a cable-stayed bridge girder is an informative indicator of structural conditions and its normal variation induced by the environment factors must be first ascertained in order to achieve more reliable structural evaluation. In this study, we used the SHM data of the Shanghai Yangtze River Bridge to investigate the mechanisms of the thermally induced vertical deflection at mid-span (D_T) by FE analysis. The findings of the study include: (1) Under normal operational conditions, the D_T variation of a cable-stayed bridge is the resultant of a multisource combination of thermal expansion effects mainly related to the cable temperature (T_{Cab}), girder

temperature (T_{Gir}), girder differential temperature (T_{Dif}), and tower temperature (T_{Tow}); and the relationships can be well approximated by a multiple linear superposition. There is no general monotonic trend between the D_T variation and the ambient temperature or the temperature of a particular structural component. (2) The thermal sensitivities of the D_T variation of the Shanghai Yangtze River Bridge to the contributory temperatures are in the following order: $T_{Cab} > T_{Gir} > T_{Tow} > T_{Dif}$. The D_T occurs downward with increasing T_{Cab}, but upward with increasing T_{Gir}, T_{Dif}, and T_{Tow}. Taking the actual temperature range into consideration, the magnitudes of the effects of the T_{Cab} and T_{Gir} are almost one order greater than those of the T_{Dif} and T_{Tow}. This mechanism can be used to explain the seasonal and daily variations of the D_T. (3) The structural temperature distribution, rather than the ambient temperature, should always be monitored along with the deformation so that the structural responses during operation can be normalized to the same temperature field to obtain a more reliable structural condition assessment.

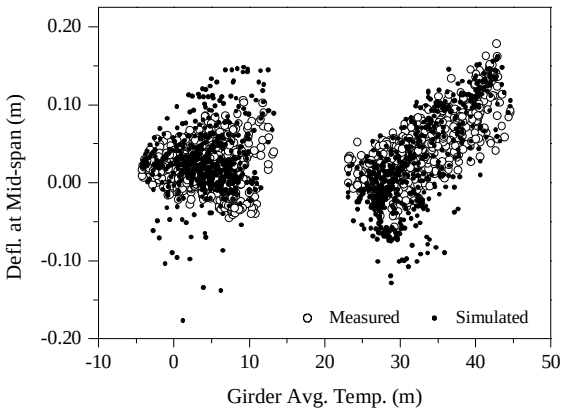

Fig. 10 D_T^a / D_T vs. T_{Gir} (February and July)

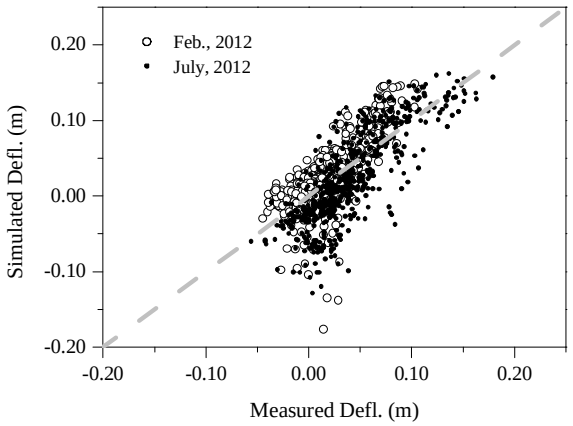

Fig. 11 D_T^a vs. D_T (February and July)

Strictly speaking, the conclusions here only aim at Shanghai Yangtze River Bridge. Further studies of the thermal effects are required for more cable-stayed bridges with different structural layouts and climatic conditions. However, the mechanisms of the thermally induced vertical deflection variation at mid-span of a cable-stayed bridge as well as the analytical methodology adopted in this study could be applicable; and the results herein provide valuable information on structural behavior interpretation.

Acknowledgments

The authors express their profound appreciation of the financial support of the National Basic Research Program of China (973 Program): Basic research on life-cycle disaster control and performance-based design of super long-span bridges (Grant No.: 2013CB036305), as well as the assistance of Shanghai Yangtze River Bridge Management Co., Ltd. and Shanghai Just One Technology Development Co., Ltd.

References

Barr, P., Eberhard, M., Stanton, J., Khaleghi, B. and Hsieh, J. C. (2000), *High performance concrete in Washington State SR18/SR516 overcrossing: final report on girder monitoring*, Washington State Transportation Center.

Boller, C., Chang, F.K. and Fujino, Y. (2009), *Encyclopedia of Structural Health Monitoring*, John Wiley & Sons, Ltd., Chichester, United Kingdom.

Brownjohn, J.M.W., Worden, K., Cross, E., List, D., Cole, R. and Wood, T. (2009), "Thermal effects on performance on Tamar Bridge", *Proceedings of the 4th International Conference on Structural Health Monitoring of Intelligent Infrastructure (SHMII-4)*, Zurich, Switzerland, July.

Burdet, O.L. (2010), *Thermal effects in the long-term monitoring of bridges*, IABSE Symposium Report, Venice, Italy, September.

Cao, Y., Yim, J., Zhao, Y. and Wang, M.L. (2011), "Temperature effects on cable stayed bridge using health monitoring system: a case study", *Struct. Health Monit.*, **10**(5), 523-537.

Catbas, F.N., Susoy, M. and Frangopol, D.M. (2008), "Structural health monitoring and reliability estimation: long span truss bridge application with environmental monitoring data", *Eng. Struct.*, **30**(9), 2347-2359.

Chen, D., Jing, G. and Huang, Z. (2006), "Prediction of bridge structural performance under temperature by artificial neural network", *Struct. Engineers*, **22**(4), 24-28. (In Chinese)

Deng, Y., Ding, Y. and Li, A. (2010), "Structural condition assessment of long-span suspension bridges using long-term monitoring data", *Earthq. Eng. Eng. Vib.*, **9**(1), 123-131.

Figueiras, J., Félix, C. and Afonso Costa, B. (2005), "Testing and monitoring of a centenary arch bridge", *Struct. Infrastruct. E.*, **1**(1), 63-73.

Gentile, C. and Saisi, A. (2013), "Long-term Dynamic Monitoring of the historic "San Michele" Iron Bridge (1889)", *Proceedings of the IABSE Spring Conference 2013*, Rotterdam, Netherlands, May.

Ghali, A., Elbadry, M. and Megally, S. (2000), "Two-year deflections of the Confederation Bridge", *Can. J. Civil Eng.*, **27**(6), 1139-1149.

Katsuchi, H., Yamada, H. and Kusuhara, S. (2008), "Structural monitoring and design verification of Akashi Kaikyo Bridge", *Proceedings of the Earth & Space 2008*, Long Beach, California, United States, March.

Kim, S., Kim, C. and Lee, J. (2005), *Monitoring results of a self-anchored suspension bridge*, Sensing Issues in Civil Structural Health Monitoring, (Ed. Ansari, F.), 475-484.

Koo, K.Y., Brownjohn, J.M.W., List, D.I. and Cole, R. (2013), "Structural health monitoring of the Tamar

Suspension Bridge", *Struct. Control Health Monit.*, **20**(4), 609-625.
Li, H., Li, S., Ou, J. and Li, H. (2010), "Modal identification of bridges under varying environmental conditions: temperature and wind effects", *Struct. Control Health Monit.*, **17**(5), 495-512.
Li, X. (2012), *Static behavior analysis of cable-stayed bridge based on long-term monitoring data*, Master Thesis, Tongji University, Shanghai.
Li, X., Ren, W. and Zhong, J. (2011), "Making good use of suspension bridge health monitoring system", *Proceedings of the 1st International Conference on Civil Engineering, Architecture and Building Materials (CEABM 2011)*, Haikou, P. R. China, June.
Magalhães, F., Cunha, A. and Caetano, E. (2012), "Vibration based structural health monitoring of an arch bridge: From automated OMA to damage detection", *Mech. Syst. Signal Pr.*, **28**, 212-228.
Moorty, S. and Roeder, C. (1992), "Temperature-dependent bridge movements", *J. Struct. Eng. - ASCE* , **118**(4), 1090-1105.
Ni, Y., Xia, H., Wong, K. and Ko, J. (2011), "In-Service condition assessment of bridge deck using long-term monitoring data of strain response", *J. Bridge Eng.*, **17**(6), 876-885.
Reynders, E., Wursten, G. and De Roeck, G. (2014), "Output-only structural health monitoring in changing environmental conditions by means of nonlinear system identification", *Struct. Health Monit.*, **13**(1), 82-93.
Shao, C. (2010), "Shanghai Yangtze River Bridge—the longest Road-cum-Rail bridge in china", *J. Struct. Eng. - ASCE*, **20**(3), 291-295.
Sohn, H. (2007), "Effects of environmental and operational variability on structural health monitoring", *Philos. T. R. Soc. A*, **365**(1851), 539-560.
Sun, Z., Wu, H.S., Wang, Q.M., Lu, Y.C. and Zhou, Z.F. (2010), "Reliability assessment oriented monitoring system design for Shanghai Yangtze River Bridge", *Proceedings of the 5th International Conference on Bridge Maintenance, Safety and Management (IABMAS)*, Philadelphia, United States, July.
Wang, M.L. (2009), *Loads and temperature effects on a bridge*, Encyclopedia of Structural Health Monitoring, (Eds., Boller, C., Chang, F. and Fujino, Y.), John Wiley & Sons, Ltd.
Wenzel, H. (2009), *The influence of environmental factors*, Encyclopedia of Structural Health Monitoring, (Eds., Boller, C., Chang, F. and Fujino, Y.), John Wiley & Sons, Ltd.
Westgate, R.J. (2012), *Environmental effects on a suspension bridges performance*, Ph.D. Dissertation, The University of Sheffield, Sheffield.
Xia, Y., Chen, B., Weng, S., Ni, Y. and Xu, Y. (2012), "Temperature effect on vibration properties of civil structures: a literature review and case studies", *J. Civil Struct. Health Monit.*, **2**(1), 29-46.
Xia, Y., Chen, B., Zhou, X. and Xu, Y. (2013), "Field monitoring and numerical analysis of Tsing Ma Suspension Bridge temperature behavior", *Struct. Control Health Monit.*, **20**(4), 560-575.
Xu, Y.L., Chen, B., Ng, C.L., Wong, K.Y. and Chan, W.Y. (2010), "Monitoring temperature effect on a long suspension bridge", *Struct. Control Health Monit.*, **17**(6), 632-653.
Zhu, Y., Fu, Y., Chen, W. and Huang, S. (2006), "Online deflection monitoring system for Dafosi Cable-stayed Bridge", *J. Intel. Mat. Syst. Str.*, **17**(8-9), 701-707.